doi:10.1016/j.jmb.2006.11.002 *J. Mol. Biol.* (2007) **365**, 1545–1558

JMB

Available online at www.sciencedirect.com

ScienceDirect

ELSEVIER

Crystal Structures of a Poxviral Glutaredoxin in the Oxidized and Reduced States Show Redox-correlated Structural Changes

John-Paul Bacik and Bart Hazes*

Department of Medical Microbiology and Immunology 1-15 Medical Sciences Building University of Alberta Edmonton, Alberta Canada T6G 2H7

**Corresponding author*

Glutaredoxins act as reducing agents for the large subunit of ribonucleotide reductase (R1) in many prokaryotes and eukaryotes, including humans. The same relationship has been proposed for the glutaredoxin and R1 proteins expressed by all orthopoxviruses, including vaccinia, variola, and ectromelia virus. Interestingly, the orthopoxviral proteins share 45% and 78% sequence identity with human glutaredoxin-1 (Grx-1) and R1, respectively. To study structure-function relationships of the vertebrate Grx-1 family, and reveal potential viral adaptations, we have determined crystal structures of the ectromelia virus glutaredoxin, EVM053, in the oxidized and reduced states. The structures show a large redox-induced conformational rearrangement of Tyr21 and Thr22 near the active site. We predict that the movement of Tyr21 is a viral-specific adaptation that increases the redox potential by stabilizing the reduced state. The conformational switch of Thr22 appears to be shared by vertebrate Grx-1 and may affect the strictly conserved Lys20. A crystal packing-induced structural change in residues 68–70 affects the GSH-binding loop, and our structures reveal a potential interaction network that connects the GSH-binding loop and the active site. EVM053 also exhibits a novel *cis*-proline (Pro53) in a loop that has been shown to contribute to R1-binding in *Escherichia coli* Grx-1. The *cis*-peptide bond of Pro53 may be required to promote electrostatic interactions between Lys52 and the C-terminal carboxylate of R1. Finally, dimethylarsenite was covalently attached to Cys23 in one reduced EVM053 structure and our preliminary data show that EVM053 has dimethylarsenate reductase activity.

Keywords: glutaredoxin; poxvirus; arsenate reductase; ribonucleotide reductase; glutathionylation

Introduction

Glutaredoxins and thioredoxins form a structurally and functionally related family of small redox proteins that play important roles in the reduction of protein disulfides, mixed disulfides, and other redox reactions.[1] Catalysis by thioredoxins and most glutaredoxins relies on two catalytic cysteine residues that cycle between reduced (dithiol) and oxidized (disulfide) states. Both enzyme families receive their reducing power from the cellular NADPH pool in slightly different ways. Thioredoxin reductase directly couples the two-electron oxidation of NADPH to the two-electron reduction of thioredoxin. In contrast, glutaredoxins are typically reduced by two molecules of reduced glutathione (GSH), which are concomitantly oxidized

Abbreviations used: Grx, glutaredoxin; EVM, ectromelia virus strain Moscow; GSH, reduced glutathione; GSSG, oxidized glutathione; DTT, dithiothreitol; MPD, 2-methyl-2,4-pentanediol; GST, glutathione *S*-transferase; RNR, ribonucleotide reductase; DMA-3, dimethylarsenite; DMA-5, dimethylarsenate; MMA, monomethylarsenate; dNTP, deoxyribonucleotidetriphosphate; NDP, ribonucleotidediphosphate; dNDP, deoxyribonucleotidediphosphate; RMSD, root mean square deviation.

E-mail address of the corresponding author: Bart.Hazes@Ualberta.ca

to a glutathione disulfide (GSSG). NADPH then reduces GSSG back to two GSH molecules in a reaction catalyzed by glutathione-reductase. Monothiol glutaredoxins form a special subclass with only one catalytic cysteine. In these enzymes, the intramolecular nucleophilic attack by the second active site cysteine is replaced with an inter-molecular attack by GSH or other external thiol.[1] This liberates the mixed disulfide reaction intermediate and restores the enzyme to its reduced state.

Thioredoxins have a very low redox potential (−270 mV for *Escherichia coli* thioredoxin[2]), which makes them efficient catalysts for the reduction of disulfides in other proteins. Glutaredoxins have a higher redox potential (−198 to −233 mV[3]) and they reduce general protein disulfides with lower efficiency.[4] However, glutaredoxins have been described as reducing agents for a few specific targets that rely on disulfide formation and reduction during catalysis. Examples include ribonucleotide reductase[5] and arsenate reductase.[6] A different role for glutaredoxins appears to be the reduction of mixed disulfides between glutathione and other thiols, including protein cysteine residues.[4,7] Glutathionylation of cysteine residues on proteins has been recognized as an important post-translational regulatory system that responds to oxidative stress by sensing the cellular GSSG:GSH ratio.[8] The implication of glutaredoxins in redox-sensitive regulatory roles has placed new emphasis on the need to better understand catalysis and substrate specificity determinants for this class of proteins.

Poxviruses are double-stranded DNA viruses with large genomes that encode many of the genes needed for DNA replication and nucleotide metabolism.[9] Sequencing of many poxvirus genomes has shown that all of them conserve one glutaredoxin-like gene that is involved in the maturation of viral capsid proteins[10] and for which the structure was recently determined.[11] Another glutaredoxin gene is found exclusively in the orthopoxviruses, the family that includes the medically most important viruses such as smallpox, vaccinia, and monkeypox.[12] This gene (named O2L in vaccinia) shares the highest level of sequence identity with the human cytoplasmic glutaredoxin Grx-1 (45% identity). The orthopoxvirus genomes also encode ribonucleotide reductase (RNR) R1 and R2 genes that share 76% and 80% sequence identity with their mammalian orthologs, respectively. The fact that the RNR R1 subunit is a known substrate for many glutaredoxins suggests that the viral glutaredoxin may be the reducing agent for the viral RNR. However, there are arguments both for and against such a role. Experimental support comes from a study with knockout vaccinia viruses lacking either O2L or the viral RNR R1 subunit. In cells pretreated with α-amanitin, an inhibitor of host but not viral transcription, both recombinant viruses caused similar defects in nucleotide metabolism, suggesting that R1 and O2L participate in the same metabolic pathway.[13] Bioinformatics also supports a functional link because O2L orthologs are only found in poxviruses that also encode the RNR R1 subunit.[12,13] Moreover, we noticed that *Ectocarpus siliculosus* virus, another double-stranded DNA virus, encodes RNR R1 and R2 subunits in its genome[14] with the R2 subunit having a glutaredoxin domain fused to its N terminus (accession code NP_077613). Gene fusion is frequently found for proteins that form a functional complex.[15] The arguments against a role for O2L as an RNR reducing factor arise from functional considerations. First, it appears highly likely that host glutaredoxin and thioredoxin can reduce the viral RNR R1 subunit. Indeed, swinepox, the only non-orthopoxvirus with a RNR R1 gene, does not encode an O2L ortholog, suggesting that it relies on host enzymes. Second, O2L is expressed as a late gene,[12] after DNA replication has started, in contrast to the early expression of all other viral genes that are involved in nucleotide metabolism.[9] This exception may be explained by the fact that O2L is packaged in the virion[12] and is thus introduced into cells upon infection.

Although the role of orthopoxviral glutaredoxins remains controversial, a comparison with the primary and tertiary structure of mammalian glutaredoxins can reveal adaptations that reflect different functional needs of the viral and mammalian enzymes. Here we present 1.8 Å resolution crystal structures of reduced and oxidized EVM053, the O2L ortholog from ectromelia virus strain Moscow (EVM). EVM is a mouse-specific orthopoxvirus that is closely related to vaccinia and smallpox, and therefore forms a suitable animal model. This is the first vertebrate-like glutaredoxin for which structures of both oxidation states have been determined. Comparisons with structures of mammalian, *E. coli*, and T4 bacteriophage glutaredoxins show unique features including the first observation of a large redox-linked structural rearrangement, a novel *cis*-proline residue, and arsenylation of Cys23. These observations generate new testable hypotheses about substrate specificity, control of redox potential, and a putative physiological role in arsenic metabolism.

Results

Model completeness and quality

EVM053 crystallizes in space group $C222_1$, with two molecules in the asymmetric unit (referred to as chains A and B). Diffraction data to 1.8 Å were obtained for both the reduced and oxidized structures and final R values are R_{cryst} = 18.3%, R_{free} = 20.8% for the reduced structure and R_{cryst} = 18.0% and R_{free} = 21.9% for the oxidized structure. For each protein model all native residues were built except the C-terminal cysteine residue for which no clear density was observed. At the N terminus, several residues from the His_6-tag demonstrated interpretable electron density. In both chains of the oxidized and reduced structures, electron density for the

residue immediately preceding the N-terminal methionine of the native protein indicated that the histidine had been mutated into a glutamate or glutamine. This residue has been built as glutamine since only glutamine can be formed from a histidine codon by a single base change. Two histidine residues preceding the glutamine were built in the A chain of both structures, while one extra histidine was built for the B chains. Throughout this article, residue numbers refer to the native EVM053 sequence. Due to lack of electron density, the side-chain atoms beyond the C^{β} position could not be modeled for Lys49 in any of the structures. The side-chains of Arg27 and Arg40 showed disorder in some but not all structures. The following residues have been modeled with dual side-chain conformations: oxidized chain A, Glu4; oxidized chain B, Gln63, Ser84, Ser100; reduced chain A, Cys23; reduced chain B, Arg58. Analysis of the Ramachandran plots computed by PROCHECK[16] shows that 98.9% (reduced structure) and 97.9% (oxidized structure) of the modeled residues are in the most favoured regions with no residues in the disallowed regions. Diffraction data, refinement statistics, and model parameters are summarized in Table 1.

Overall structure of EVM053

As expected, the overall structure of EVM053 conforms to the glutaredoxin fold, with a core of four β-strands flanked by five α-helices (Figure 1). The active site cysteine pair is located in the loop connecting the first β-strand to the second α-helix and the cysteine residues form a CPFC sequence motif. This is identical to the active site motif in pig Grx-1 and very similar to the CPYC motif in other vertebrate Grx-1 sequences.[1] The first cysteine, Cys23, is exposed to solvent whereas the second cysteine, Cys26, adopts a more buried location in the first turn of the second α-helix. A proline at position 71 forms a *cis*-peptide bond in EVM053 and all other glutaredoxins and thioredoxins of known structure.[17] This *cis*-proline induces a sharp turn in the main chain at the start of β-strand 3 and it positions the proline side-chain atoms directly beside the active site cysteine residues. Interestingly, EVM053 contains a second *cis*-proline, Pro53, at the start of the third α-helix (Figure 1). This proline is conserved in all orthopoxvirus orthologs but is not present in any other known glutaredoxin. The corresponding region in *E. coli* Grx-1 has been shown to interact with the RNR R1 C-terminal peptide,[18] suggesting a potential role for *cis*-Pro53 in substrate binding (see below).

The two EVM053 monomers per asymmetric unit form two types of dimers, one related by non-crystallographic 2-fold symmetry (585 Å^2 buried surface), the other by the crystallographic 2-fold along the *x*-axis (840 Å^2 buried surface). However, Superose 6 size-exclusion chromatography with real-time analysis of the eluent by static and dynamic light scattering (Dawn EOS/QELS, Wyatt Inc.) yielded an estimated molecular mass of 14.8 kDa (13,272 Da predicted monomer mass) and a polydispersity factor of 1.0. This confirms that, like other known Grx-1 enzymes, EVM053 is a monomer in solution.

Table 1. Diffraction data and refinement statistics

	Oxidized	Reduced
Diffraction data statistics[a]		
Space group	$C222_1$	$C222_1$
Unit cell dimensions	$a=61.98$, $b=67.57$, $c=108.55$	$a=62.63$, $b=66.67$, $c=108.10$
Resolution range (Å)	36.20–1.80 (1.90–1.80)	54.07–1.80 (1.87–1.80)
Measured reflections	113,946 (6928)	82,915 (7496)
Unique reflections	20,896 (2737)	21,297 (2305)
Completeness (%)	96.7 (88.0)	99.6 (97.3)
R_{sym}	0.135 (0.655)	0.076 (0.473)
Mean $(I)/\mathrm{sd}(I)$	10.6 (1.8)	11.5 (2.2)
B_{wilson} (Å^2)	19.2	24.6
Refinement statistics		
R-factor	0.180	0.183
R_{free}	0.219	0.208
Number of waters	149	129
Backbone average *B*-factor (Å^2)	18.3	29.0
All atoms average *B*-factor (Å^2)	21.1	32.2
RMSD bond lengths (Å)	0.022	0.019
RMSD bond angles (°)	1.772	1.845

[a] Values in parentheses indicate statistics for the highest resolution shell.

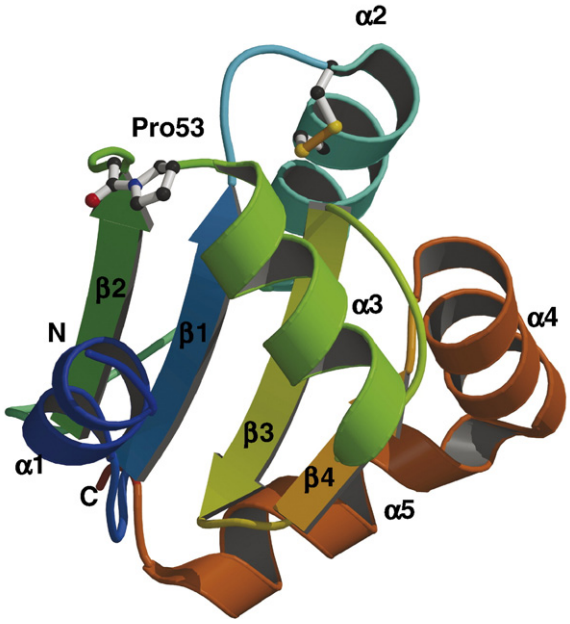

Figure 1. Cartoon representation of EVM053 in the oxidized conformation. Helices are shown as coils and strands as arrows. The disulfide bond formed by the active site cysteine residues is shown in orange and the *cis*-Pro53 is drawn in ball-and-stick format. This Figure was generated using MOLSCRIPT[67] and Raster3D.[68]

EVM053 active site structure

The A and B chains of oxidized EVM053 adopt an active site structure that is very similar to the conformation reported for oxidized pig Grx-1[19] (Table 2). The disulfide bond length refined to 2.07 and 2.10 Å for the A and B chains, respectively. This is slightly longer than the ideal value of 2.03 Å, but similar to the 2.08 Å in oxidized pig Grx-1. Electron density for the active site disulfide bond is shown in Figure 2(a). The active site structure of reduced EVM053 differs for the A and B chains. In chain A, the Cys23 side-chain displays two alternate conformations with occupancies that refined to 0.57 and 0.43 for rotamers A and B, respectively (Figure 2(b)). Rotamer A corresponds to the conformation observed in other reduced glutaredoxin structures and is also similar to the conformation of Cys23 in the B chain. Rotamer A places the Cys23 sulfur atom at 3.27 Å from the sulfur of Cys26, which is too close for a normal non-bonded interaction. Short sulfur-sulfur distances have been reported for disulfides that have been disrupted by radiation damage.[20] However, we are not aware of evidence that the same damage occurs to reduced disulfides. In addition, we did not observe other common features of radiation damage such as an increase in unit cell volume or decarboxylation of glutamic and aspartic residues, and the X-ray dose during data collection was similar to that used for the oxidized structure for which no signs of radiation damage were observed. A more likely interpretation is that the short sulfur–sulfur distance represents a thiol-thiolate hydrogen bond. Thiol-thiolate hydrogen bonds have been observed in several structures with sulfur–sulfur distances of 3.0 to 3.5 Å[21–23] and the existence of a thiol-thiolate hydrogen bond in glutaredoxins has been proposed previously.[24] In the B rotamer, the Cys23 sulfur atom points away from the active site and the distance between the active site sulfur atoms is 5.69 Å.

Electron density for chain B supports only one side-chain conformation for Cys23 with a distance of 3.82 Å between the two sulfur atoms in the active site. In this chain, additional electron density indicates that Cys23 has been covalently modified, and the density features are consistent with the addition of dimethylarsenite (DMA-3) (Figure 2(c)). We used cacodylate (dimethylarsenate, DMA-5) as our crystallization buffer and dithiothreitol (DTT) as a reducing agent. DTT is known to reduce cacodylate and the resulting DMA-3 can form stable adducts with cysteine.[25] The modeling of the extra density as DMA-3 is further supported by the fact that the arsenic density peak is larger than the density for the sulfur atom, as expected for a higher atomic number element. Moreover, the center of the extra density is located 2.4 Å from the Cys23 sulfur, too far for a disulfide bond and very similar to sulfur-arsenic bond lengths observed in other structures.[25] Finally, two methyl groups expected for DMA-3 are clearly visible in the density (Figure 2(c)). Arsenylation is not complete and the DMA-3 occupancy refined to 0.58.

Redox-state induced structural changes

Comparison of the reduced and oxidized EVM053 structures revealed a dramatic structural rearrangement of Tyr21 near the active site (Figure 3). This residue flips around, causing the main-chain C^{α} atom to move by 1.6 and 1.8 Å, while the side-chain hydroxyl moves 10.7 and 11.2 Å in the A and B chains, respectively. In the reduced conformation, the side-chain of Tyr21 is packed onto a strongly hydrophobic pocket at the surface of the protein formed by residues Val19, Leu30 and Ile45. In contrast, in the oxidized state the tyrosine side-chain is solvent-exposed. All orthopox EVM053 orthologs conserve either a tyrosine or phenylalanine at this position, consistent with a functional role for an aromatic residue. This is not the case for mammalian Grx-1, where the equivalent residue is a proline. Reduction of the active site disulfide also triggers a change in Thr22, with the main-chain oxygen moving towards the solvent, while the side-chain swivels around the C^{α}-C^{β} bond to avoid steric hindrance. As a result, Lys20 in the B chain forms a hydrogen bond with the Thr22 side-chain hydroxyl in the reduced state, instead of the hydrogen bond with the main-chain oxygen of Thr22 in the oxidized state (see right-hand side of Figure 4). Interestingly, the redox-induced change of Thr22 in EVM053 is also observed when comparing the structures of oxidized pig and reduced human Grx-1.

Structural flexibility in the GSH-binding loop

A comparison of the A and B chains showed structural differences in residues 68–70 that were observed in both the oxidized and reduced states (left-hand side of Figure 4). Although these differences appear to be due to crystal packing effects, they suggest

Table 2. Active site geometry

	Oxidized EVM053		Reduced EVM053			Pig Grx-1
Model[a]	Chain A	Chain B	Chain A^{A}	Chain A^{B}	Chain B	Oxidized
$23S^{\gamma}$-$26S^{\gamma}$ [Å]	2.10	2.07	3.27	5.69	3.82	2.08
$23S^{\gamma}$-25N [Å]	4.48	4.38	3.86	5.13	3.41	4.20
$23S^{\gamma}$-26N [Å]	3.32	3.25	3.41	5.77	3.62	3.34
23 Chi1 [°]	150.0	166.2	169.7	−129.8	171.8	167.8

[a] Chain A and chain B represent the two EVM053 monomers that are present in the asymmetric unit of the crystals. Superscript A and B indicate the alternate side-chain conformations of Cys23 in the A chain model of the reduced crystals.

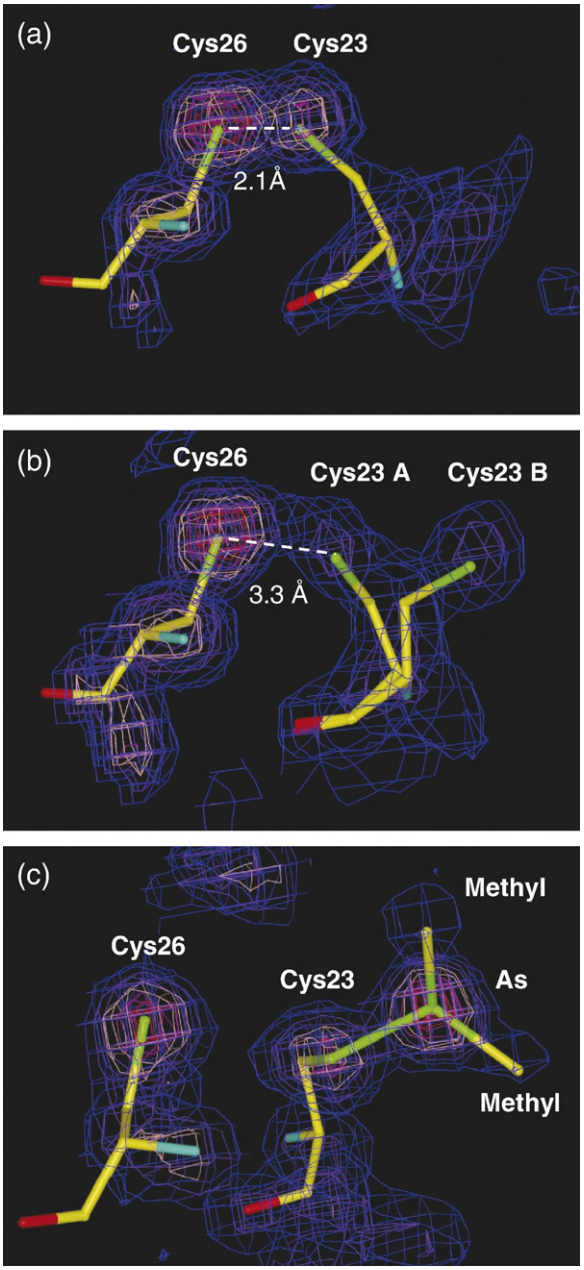

Figure 2. Electron density ($2\,|F_{obs}| - |F_{calc}|$) for the active site of EVM053 in the (a) oxidized; (b) reduced; (c) dimethylarsenylated states. The disulfide bond in the oxidized structure and the proposed hydrogen bond in the reduced structure are indicated by broken lines. This Figure was generated using Xfit[65] and Raster3D.[68]

structural flexibility of this region, which is of interest since Thr69 and Val70 are highly conserved residues that have been shown to contribute to GSH binding in published Grx-GSH complex structures.[17,26,27] In the A chain, Thr69 is tilted towards the active site, which would interfere with GSH binding. In chain B, the GSH-binding loop corresponds more closely to that observed for other glutaredoxins, including structures in complex with bound GSH (see below).

The deviating conformation of the residue 68–70 loop in the A chain may be related to the presence of an arginine at position 58, a residue that is strictly conserved as a glutamine in all vertebrate Grx-1 and Grx-2 sequences. Structures of GSH in complex with human Grx-1[26] and human Grx-2 (PDB code 2FLS, C. Johansson *et al.*, unpublished results) show that the conserved glutamine forms a hydrogen bonding network with the strictly conserved Lys20 (Lys34 in Grx-2), the C-terminal carboxylate of GSH, and the main-chain carbonyl oxygen of residue 68 (Arg79 in Grx-2; Figure 5(a)). The Arg58 side-chain of EVM053 cannot make an equivalent hydrogen bond with Lys20. In contrast, electrostatic repulsion will drive the two positively charged residues apart. In chain A, this electrostatic repulsion is avoided by a more exposed conformation of Arg58 that places its positive side-chain far from Lys20 (yellow model in Figure 4). In this conformation, the main-chain carbonyl oxygen of residue 68 is not stabilized by a hydrogen bond, which may affect the position of Thr69. In the oxidized B chain, Arg58 adopts a conformation more similar to that of the conserved glutamine, including the stabilizing hydrogen bond to the main-chain carbonyl oxygen of residue 68 (green model in Figure 4). In this case the electrostatic repulsion causes an alternate conformation of the Lys20 side-chain, which places its positive charge closer to the active site and within hydrogen bonding distance of Thr22.

Model for the EVM053-SG complex

NMR structures of glutaredoxins with a glutathionylated active site cysteine have been published for

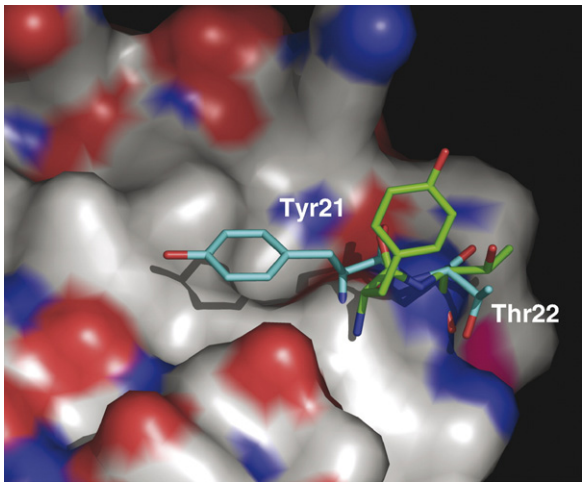

Figure 3. Structural changes due to redox state. Side-chain conformations of Tyr21 and Thr22 in the reduced (cyan) and oxidized (green) B chain states are shown. Equivalent structural changes exist in the A chain models. The molecular surface representation of the reduced B chain is shown to demonstrate that Tyr21 is stabilized by interactions with a hydrophobic pocket formed by residues Val19, Ile30 and Ile45. In the oxidized state Tyr21 is exposed to solvent. Oxygen, nitrogen, and carbon atom surfaces are rendered in red, blue, and grey, respectively. This Figure and all subsequent Figures were generated using PYMOL.[69]

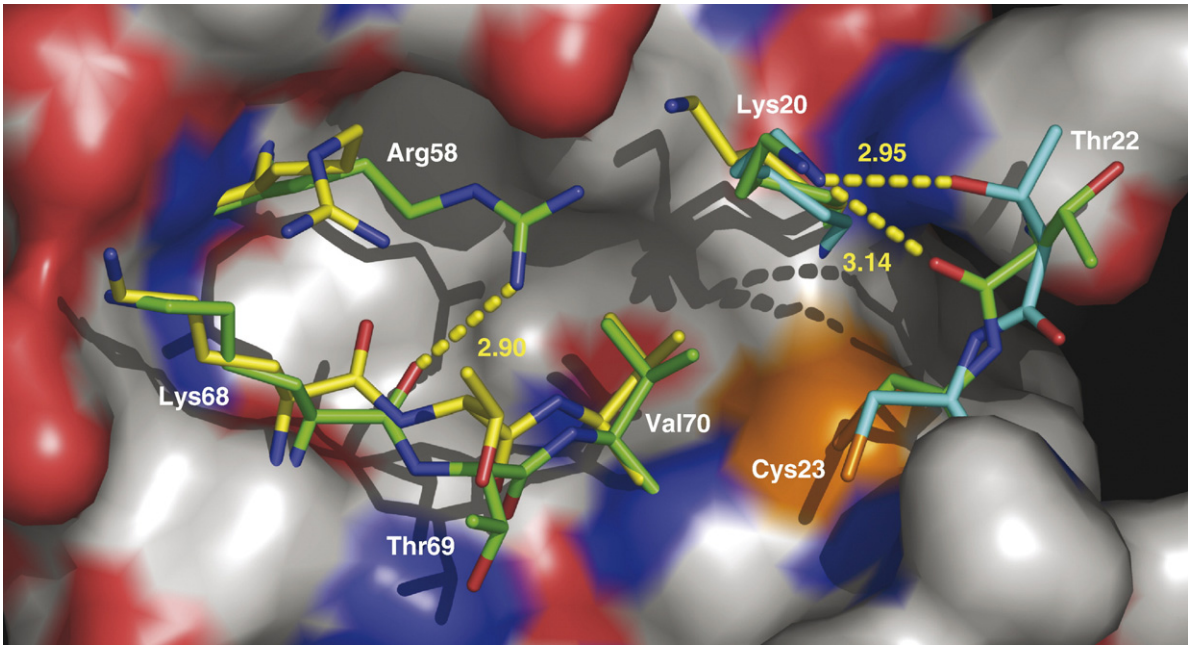

Figure 4. Structural changes in the GSH-binding loop and potential structural cross-talk with Thr22. Side-chains demonstrating alternate conformations are shown in yellow (oxidized A), green (oxidized B), and cyan (reduced B). The side-chain of Arg58 adopts a more buried side-chain conformation in chain B that is stabilized by a hydrogen bond to the main-chain carbonyl oxygen of Lys68. The Lys20 side-chain moves closer to the active site in chain B, likely due to electrostatic repulsion by Arg58. Thr22 forms different hydrogen bonds with the B chain conformation of Lys20 depending on the oxidation state. Hydrogen bonds are indicated by yellow broken lines, with atomic distances in angstroms.

E. coli Grx-1[27] and Grx-3,[17] as well as human Grx-1.[26] A human Grx-2-GSH complex crystal structure has also been deposited (PDB code 2FLS, C. Johansson *et al.*, unpublished results). In all structures, the GSH-cysteine residue makes antiparallel β-sheet-like hydrogen bonds with the amide nitrogen and carbonyl oxygen of Val70. We have modeled GSH binding to EVM053 based on the human Grx-2-GSH crystal structure, which shows clear electron density for the bound glutathione with favourable interactions between the γ-glutamyl backbone carboxylate and the N-terminal end of α-helix 4. In the Grx-2-GSH model, the distance between the thiols of the nucleophilic active site cysteine and GSH is 2.83 Å, suggesting that GSH is bound as a non-covalent complex and likely forms a thiol-thiolate hydrogen bond. Figure 5(a) and (b) shows the experimental Grx-2-GSH complex structure and the EVM053 B chain with a model of bound GSH. To make the EVM053-GSH model, we superimposed the Grx-2-GSH structure onto the reduced EVM053 B chain by optimizing the fit between all main-chain atoms of residues 20 to 26, 68 to 70, and 82 to 84 of EVM053 and the corresponding atoms of Grx-2 (52 atoms matched with an RMSD of 0.38 Å). We used the program SSBOND[28] to create a stereochemically optimal mixed disulfide bond. Interestingly, four residues that contribute to GSH-binding in Grx-2 (Lys34, Gln69, Thr80 and Thr95) have different conformations in the corresponding residues of the EVM053 A and B chains (Lys20, Arg58, Thr69 and Ser84). There is a steric conflict between the GSH-glycine and Thr69 in the GSH-binding loop of the A chain. A conformational change of this loop towards a more Grx-2-like conformation is needed to accommodate GSH and such a rearrangement is actually observed in the B chain. Residues Lys20 and Ser84 will most likely also adopt Grx-2-like conformations upon GSH binding. We predict that Arg58 will adopt the exposed conformation shown in pink in Figure 5(b). This conformation can make a salt-bridge interaction with the GSH-glycine carboxylate and avoids an electrostatic conflict with Lys20.

Implications for the binding of R1

The NMR structure of *E. coli* Grx-1 in complex with a peptide representing the C-terminal 25 residues of *E. coli* RNR R1 has been determined.[18] This structure represents the covalent intermediate of disulfide reduction by glutaredoxin with a mixed disulfide between Cys11 of the enzyme and Cys759 of the peptide (Cys14 and Cys754 were mutated to serine to obtain a stable complex). Only the C-terminal ten residues of the peptide were well-ordered and electrostatic complementarity between the anionic peptide and cationic peptide-binding groove, including four salt-bridges, was proposed to be a major determinant of binding.[18] However, R1 and Grx-1 sequences from mammals and orthopoxviruses do not appear to conserve these salt-bridges, with the possible exception of a salt-bridge to the C-terminal carboxylate of the peptide. In *E. coli*, the R1 C-terminal residues that follow the reactive cysteine

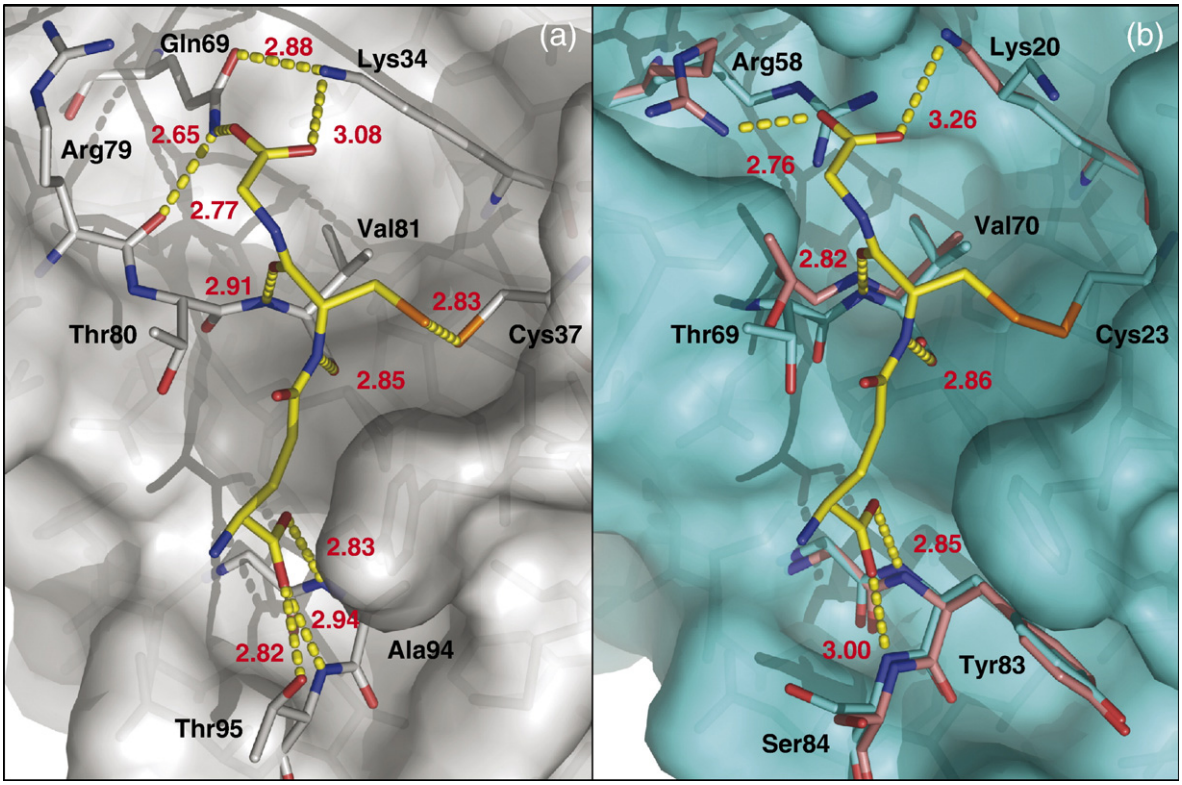

Figure 5. GSH binding to Grx-2 and EVM053. GSH is shown in yellow and residues involved in GSH-binding are drawn in stick format. Proposed hydrogen bonds are indicated by broken lines and atomic distances are given in angstroms. (a) Experimental crystal structure of the Grx-2-GSH complex. The distance of 2.83 Å between the thiols of the nucleophilic active site cysteine and GSH suggests that GSH is bound as a non-covalent complex in this structure. (b) Computer model of the reduced EVM053 B chain (cyan molecular surface representation) with GSH positioned based on the Grx-2-GSH complex structure. This complex was modeled as a covalent mixed-disulfide intermediate, which is indicated by a filled orange bond. Positions of the GSH-binding residues are shown for both the A (pink) and B (cyan) chain conformations. For EVM053 in the GSH-bound state, it is predicted that Thr69 adopts the B chain conformation, while Arg58 and Lys20 adopt the A chain conformation. Although the side-chain terminus of Ser84 is too far to form a hydrogen bond with GSH in either conformation, a small rotation of this side-chain could allow a hydrogen bond once GSH is bound.

(Lys760-Ile761) extend towards the loop following the second β-strand of Grx-1, and the C-terminal carboxylate makes a salt-bridge with Arg39 at the start of the loop (Figure 6(a)). In orthopoxviruses the R1 sequence terminates in a Ser-Gly dipeptide, and Lys49 of EVM053 is structurally equivalent to Arg39 (Figure 6(a) and (b)). In our structure the side-chain of Lys49 is disordered beyond the C^{β} atom but its position is compatible with a role in R1-peptide binding. Mammalian Grx-1 sequences do not conserve a basic residue that corresponds to Arg39 of *E. coli* Grx-1.

Figure 6(b)–(d) shows the loop between β-strand 2 and α-helix 3 in EVM053, human Grx-1 and pig Grx-1, respectively. The predicted location of the R1-peptide is indicated by the Cys-Lys-Ile tripeptide that has been positioned based on the *E. coli* Grx-1-R1 complex structure. Interestingly, this loop is the region where the main-chain conformation of EVM053 deviates most from the human and pig Grx-1 structures. This deviation is due to the *cis*-peptide bond formed by Pro53, which tilts Lys52 more towards the C terminus of the R1-peptide. Upon R1-peptide binding, Lys52 could adopt a conformation that stabilizes the negative carboxylate of the peptide. In human Grx-1, His53 is the only basic residue in the loop region that could form a salt-bridge with the R1-peptide carboxylate, although it would require some conformational rearrangements. In contrast, pig Grx-1 has no basic residues in the loop and Asp53 is not compatible with a role in R1 peptide binding.

Discussion

Our work shows a high level of structural conservation between EVM053 and the Grx-1 of humans and pig. Based on the sequence and structural similarities, the EVM053 structures can be used to complement the limited available knowledge for the orthologous mammalian enzymes. In particular, our work represents the first example where high-resolution crystal structures of both the reduced and oxidized states have been determined. At the same time, the stable integration of a host enzyme into the orthopoxvirus genome makes it likely that the viral enzyme has acquired virus-specific adaptations. Our structural studies aim to increase our

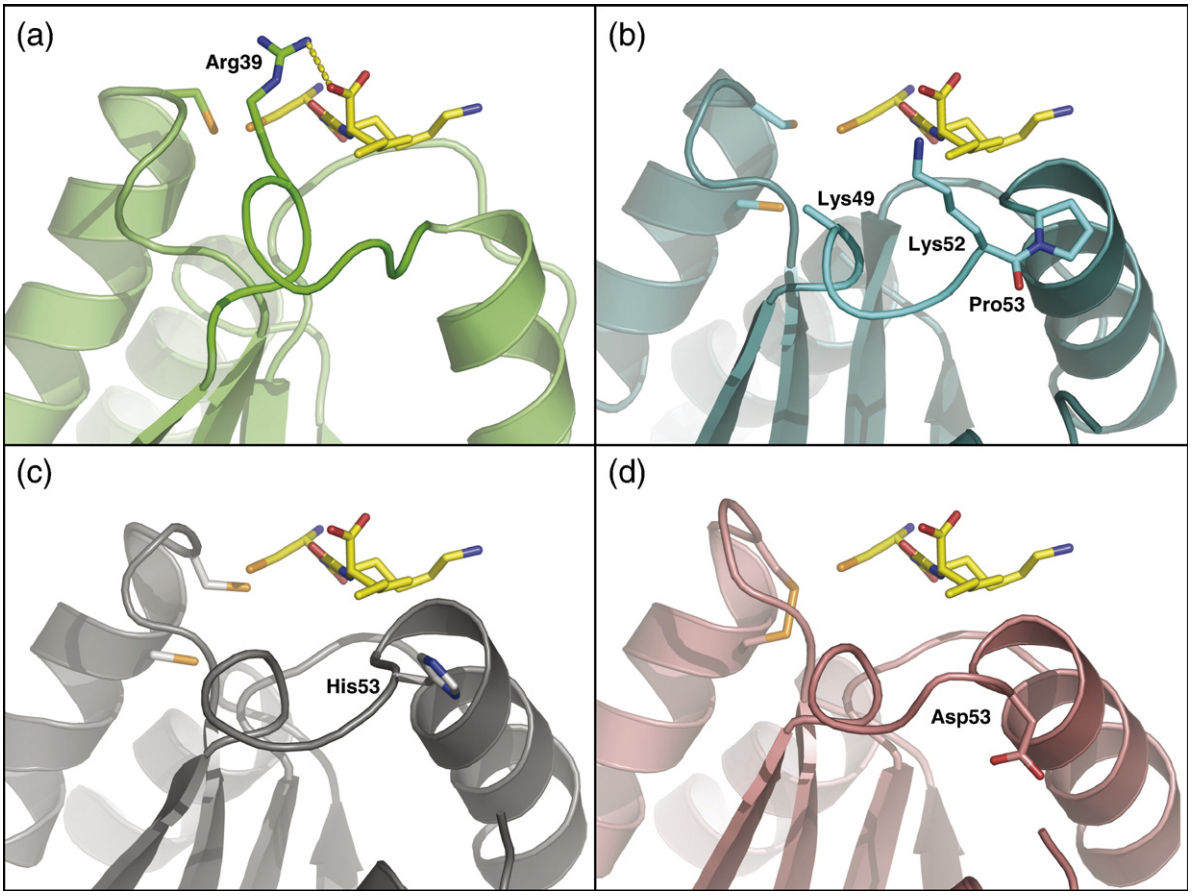

Figure 6. Proposed role of the Grx β2-α3 loop in binding of the R1 peptide substrate. Functionally important residues in the β2-α3 loop and the active site cysteine residues are shown in stick format. (a) Experimental NMR model of *E. coli* Grx-1 in complex with the R1 peptide for which the C-terminal three residues (Cys-Lys-Ile) are shown in yellow. A salt-bridge between Arg39 and the C-terminal carboxylate of R1 is demonstrated by a broken line. (b), (c), and (d) The EVM053, human Grx-1, and pig Grx-1 structures in the same orientation as the *E. coli* Grx-1 model. The anticipated location for the Cys-Ser-Gly tripeptide of orthopoxviral R1 and the Cys-Gly-Ser tripeptide of mammalian R1 is indicated by the superimposed R1 tripeptide from the *E. coli* Grx-1-mixed disulfide structure. The Lys49 side-chain in EVM053 could not be modeled beyond the C^{β} position, and only the C^{α}-C^{β} bond is shown to indicate its location.

understanding of glutaredoxins in general and delineate the features that may be virus-specific adaptations.

Cysteine-activation by thiolate stabilization

Efficient nucleophilic attack by the active site cysteine requires that the thiol is deprotonated to the thiolate state. To facilitate this, thioredoxin-fold enzymes stabilize the thiolate form as evidenced by a depressed pK_a value. Stabilization of the thiolate also affects the equilibrium between oxidized and reduced states, with greater stabilization favouring the reduced state and thus increasing the redox potential. Compared to thioredoxins, glutaredoxins have a lower pK_a and, as expected, a higher redox potential. A similar situation occurs for *E. coli* DsbA, a thioredoxin-fold enzyme involved in disulfide formation, which has a very low pK_a and very high redox potential. For DsbA, much of the pK_a depression and redox potential elevation has been attributed to the electrostatic stabilization of the Cys28 thiolate by His30.[29] For glutaredoxins, multiple factors are believed to contribute to thiolate stabilization, including nearby positively charged residues,[19] hydrogen bonding between the thiolate and main-chain amide nitrogen atoms at the start of α-helix 2,[30,31] hydrogen bonding between the thiolate and the thiol of the second active site cysteine,[24] and influences of the dipole moment of α-helix 2.[19] In our structures, positively charged residues in the vicinity of the active site (Lys20, Arg27, Arg58) are not close enough to form effective electrostatic interactions with the thiolate anion. Lys20 could adopt a conformation that brings it in contact with the thiolate and this has been proposed for human Grx-1 based on computational models.[32] However, when these authors replaced the lysine by glutamine or leucine there was essentially no effect on the pK_a value, which argues against a significant role for Lys20 in lowering the pK_a. Our structure does support the proposed thiolate stabilization by the helix-dipole, hydrogen bonding to the amide nitrogen atoms of Phe25 and Cys26, and the formation of a thiol-thiolate hydrogen bond (Table 2). Stabilization by a thiol-thiolate hydrogen bond is

also supported by the observation that mutating the second active site cysteine in human Grx-1 increases the pK_a by 0.6 units.[32]

We believe that our observation of dual side-chain conformations for Cys23 in chain A is an artefact of the crystal-mounting conditions. The crystals were grown in mother liquor with a pH of 5.2 but to obtain the reduced structure 50 mM of GSH in its free acid form was added. Subsequent measurements show that this reduces the pH to 3.6, which is close to the pK_a value for other glutaredoxins. Accordingly, Cys23 may have been partially protonated such that the short sulfur-sulfur conformation represents a thiol-thiolate hydrogen bond and the other conformation represents a non-physiological thiol form of Cys23. It seems plausible that crystal packing interactions, in particular Asp93 and the negative helix dipole moment of α-helix 4 in a neighbouring monomer, make Cys23 in the A chain more sensitive to protonation by raising the pK_a of this residue. This could also explain the preferential arsenylation of Cys23 in the B chain.

GSH binding to Grx

Oxidized Grx reacts with GSH to form a Grx-SG mixed disulfide, and reduced Grx forms the same mixed disulfide when it reacts with GSSG or a variety of glutathione mixed disulfides (RSSG), including glutathionylated proteins. Specificity for glutathione-containing substrates has been demonstrated in several studies[7,33,34] and K_m values for RSSG substrates in the low micromolar to low millimolar range have been reported.[35]

Three published NMR structures have addressed the structural basis for GSH binding to human Grx-1,[26] *E. coli* Grx-1,[27] and *E. coli* Grx-3.[17] However, discrete differences between the observed binding geometries left it unclear how EVM053 might bind to glutathione. Interestingly, a crystal structure of human Grx-2 complexed to glutathione has recently been deposited in the Protein Data Bank (PDB code 2FLS, C. Johansson *et al.*, unpublished results). In this complex, the GSH-cysteine binding mode is very similar to that of the *E. coli* Grx-3 complex, but the γ-glutamyl moiety adopts a different conformation that results in highly favourable interactions between the γ-glutamyl carboxylate and the dipole of α-helix 4. Hydrogen bonds are formed with two main-chain nitrogen atoms at the start of that helix (residues 94 and 95) and the side-chain hydroxyl of Thr95 (Figure 5(a)). In EVM053 and all orthopoxviral orthologs Ser84 is structurally and functionally equivalent to Thr95 of human Grx-2. Accordingly, we have modeled the EVM053-SG mixed disulfide based on the human Grx-2-GSH complex structure.

Thiol-disulfide interchange reactions are believed to involve an S_N2 transition state, which favours an in-line attack of the sulfur-sulfur bond by a thiolate nucleophile.[36] In agreement, the thiols of Cys26, Cys23, and GSH are approximately co-linear (152°). To make GSH a better nucleophile one would further expect Grx to stabilize the thiolate form of GSH. This is the case for glutathione *S*-transferases (GSTs) where interactions with serine, tyrosine, or arginine residues lower the pK_a of bound GSH.[37] For glutaredoxins, the conserved Lys20 could in principle stabilize a GSH-thiolate anion but in Grx-SG complex structures this lysine forms a salt-bridge with the GSH-glycine carboxylate. This places the lysine side-chain far from the active site. However, the GSH sulfur is approximately in-line with the axis of α-helix 2 and the helix dipole may thus assist thiolate formation. γ-Glutamylcysteine is a much better substrate for Grx than cysteinylglycine,[33,34] which agrees with the observation that the γ-glutamyl moiety makes more extensive interactions with the protein than the glycine moiety. However, Grx still favours GSH over γ-glutamylcysteine, indicating that the glycine residue does contribute to activity.[7] This may be due to enhanced affinity through the salt-bridges formed between Grx and the GSH-glycine carboxylate or due to destabilization of the thiolate form of γ-glutamylcysteine resulting from the closer proximity of the negatively charged terminal carboxylate on the cysteine residue.

The two EVM053 monomers in the asymmetric unit of our crystals show different conformations of the GSH-binding loop. The A chain conformation precludes GSH binding due to steric hindrance by Thr69. In the B chain, Thr69 has moved partially towards the position observed in the human Grx-2-GSH complex structure. At this moment it is not clear if the GSH-loop conformation in the A chain represents a functionally relevant conformation. This deserves further research because the Lys20 and Arg58 residues can potentially couple the oxidation state of the active site, as sensed by the Lys20-Thr22 interaction, to occupation of the GSH-binding site, as sensed by the Arg58 interaction with the main-chain carbonyl oxygen of residue 68 (Figure 4).

Ribonucleotide reductase binding to EVM053

Glutaredoxins from both mammals and *E. coli* have varying abilities to act as cofactors of RNR.[17,38] For example, Grx-3 of *E. coli* shows only 5% activity as a reductant of RNR compared to Grx-1.[18] For mammals, Grx-1 from human and calf can support RNR activity, whereas the closely related enzymes from pig and rabbit cannot.[5,39,40] We are not aware of direct experimental data showing that poxviral Grx-1 stimulates activity of the poxviral RNR. However, we have demonstrated that EVM053 can reduce oxidized decapeptides corresponding to the C-terminal sequence of mouse and ectromelia R1 (data not shown). Moreover, experiments suggesting that EVM053 acts as a reducing agent for poxviral RNR[13] imply that it binds the C-terminal peptide of the poxviral R1.

To explain the different R1 specificity of human and calf Grx-1 compared to the pig and rabbit enzyme we looked for residues in the peptide-binding groove that are not conserved between these species. The only sequence difference that

correlates with specificity is in the β2-α3 loop where pig and rabbit have an aspartate at position 53, compared to asparagine and histidine for bovine and human Grx-1, respectively. In the *E. coli* Grx-1-R1 complex structure this loop adopts a different conformation than in the native enzyme, which allows residue Arg39 to make a salt-bridge with the C-terminal carboxylate of the peptide. His53 in human Grx-1 could make a similar favourable electrostatic interaction, whereas Asn53 in bovine Grx-1 could stabilize the C terminus by hydrogen bonding. In contrast, Asp53 in pig and rabbit Grx-1 cannot interact favourably with the C-terminal carboxylate of the peptide (Figure 6).

The orthopoxvirus Grx-1 sequences have acquired two basic residues in this loop that are not found in mammalian Grx-1 and that may stabilize R1 peptide binding. Lys49 is structurally equivalent to Arg39 of *E. coli* Grx-1. The second basic residue, Lys52, does not correspond to a basic residue in other glutaredoxins but it is again close enough to form a salt-bridge with the R1 peptide C terminus. The observation that Pro53 adopts the less common *cis*-proline conformation in EVM053 is likely also relevant for function because the *cis*-peptide bond tilts Lys52 towards the R1 peptide. Mutagenesis studies of Lys49, Lys52 and Pro53 are needed to confirm a role in peptide binding for these residues.

Redox-correlated conformational changes

The natural glutaredoxin catalytic cycle has three clear structural states of the active site; fully oxidized, glutathione mixed disulfide, and fully reduced. Comparison of oxidized and reduced T4 bacteriophage glutaredoxin showed increased flexibility in the active site loop for the latter, but no clear conformational changes.[41] The same lack of redox-correlated conformational changes has been reported for other glutaredoxins.[42] For human and *E. coli* Grx-1, comparison of structures for the GSH mixed disulfide complex and the reduced state also did not show significant differences beyond changes in the active site itself. In contrast, the high-resolution NMR structures for the oxidized and GSH mixed disulfide states of *E. coli* Grx-3, showed a shift in the position of α-helix 1 and a concerted change in the side-chain rotamers of Tyr13 and Asp66.[42] This change moves Tyr13 from a highly solvent-exposed conformation in the oxidized state to a more buried conformation in the glutathionylated complex. The authors argue that the partially buried position of Tyr13 would specifically stabilize the mixed disulfide state and thus increase substrate affinity.[42]

A comparison between oxidized and reduced EVM053 structures shows a large conformational change of a different tyrosine, Tyr21, which moves the aromatic side-chain from a hydrophobic pocket in the reduced state into a fully solvent-exposed conformation in the oxidized state (Figure 3). The energetically less favourable exposed conformation in the oxidized structure can be expected to raise the redox potential of EVM053. Direct measurement of the redox potential for native EVM053 and Tyr21-Ala mutants are needed to test this structure-based hypothesis. A second, and not necessarily mutually exclusive, hypothesis is that the oxidation-state dependent conformation of Tyr21 signals the redox state of the enzyme. For instance, in the reduced state the conformation of Tyr21 may facilitate interaction between EVM053 and substrates that need to be reduced. Similar redox state-dependent binding has been described for *E. coli* thioredoxin, for which only the reduced state binds to T7 bacteriophage polymerase.[43] Although Tyr21 appears to be too far from the substrate binding groove to directly interact with the R1 C-terminal peptide or GSH, it remains a distinct possibility that this residue, and the strongly hydrophobic pocket that becomes exposed upon oxidation, may be required for interactions with other potential binding partners.

Redox stress during poxvirus genome replication

The Tyr21 conformational change mentioned above could be an adaptation to raise the redox potential of EVM053. This may be directly relevant for poxviruses because they replicate their genomes in small membrane-encapsidated vesicles referred to as virosomes.[44] To create thousands of genome copies, each ~200,000 bp long, in the period of about a day requires a high rate of dNTP production. The rate-limiting step in dNTP production is the reduction of NDP to dNDP by RNR[45] in a process that consumes two GSH and produces one GSSG for each dNDP produced. Interestingly, RNR has been reported to be recruited to virosomes[46] where its high activity could be expected to raise the local GSSG/GSH ratio. In a more oxidizing environment a higher redox potential for the viral glutaredoxin would be needed to ensure that a large fraction of the enzyme exists in the active reduced state. A related adaptation may be the loss of three non-catalytic cysteine residues that are conserved in most mammalian Grx-1 enzymes (Cys8, Cys79, and Cys83 in human Grx-1), which have been proposed to play a redox-sensitive regulatory role.[31] Cys8 and Cys79 are surface-exposed and oxidation of Cys8 has been shown to decrease the lifetime of human Grx-1 due to disulfide-linked aggregate formation.[47] Moreover, oxidation of calf thymus glutaredoxin has been shown to inhibit enzyme activity.[48] Cys83 is located in the substrate-binding groove at the N-terminal end of α-helix 4 where chemical modification of its thiol is likely to block access to the substrate-binding groove.[31] In addition, the helix dipole can reduce the pK_a of Cys83, making it more sensitive to oxidation by reactive oxygen species or glutathionylation.[31] Mutation of the cysteine residues could thus be a poxviral adaptation to avoid inhibition in an oxidizing environment. Our model predicts that all poxviruses will experience redox

stress during genome replication, yet only the orthopoxviruses express a Grx-1 ortholog. Although it is possible that other poxviruses have evolved alternative adaptations, it is tempting to speculate that the Grx-1 ortholog is needed by orthopoxviruses because they have the highest known rate of genome replication.[49] Moreover, the late expression of the orthopox Grx-1 can be explained by the fact that rates of DNA synthesis do not peak until several hours after initiation of genome replication.

Glutaredoxin role in arsenic metabolism

Trivalent arsenic compounds are known inhibitors of glutathione-utilizing enzymes, including glutathione reductase, glutathione peroxidase, and GST.[50] To our knowledge, arsenic has not been shown to inhibit glutaredoxin but the covalent modification of Cys23 by DMA-3 in our reduced EVM053 structure suggests that the glutaredoxin active site is a target for arsenic compounds. Interestingly, although trivalent arsenic inhibits GSTs, human omega class GSTs, hGSTO1-1 and hGSTO2-2, have been shown to reduce monomethyl and dimethyl arsenate.[51] Moreover, omega class GSTs display properties typical of glutaredoxins, including dehydroascorbate reductase and thioltransferase activities,[51] a catalytic cysteine (Cys32) in a glutaredoxin-like CPF sequence motif, thiolate stabilization through a helix dipole, and formation of a mixed disulfide with GSH.[52] This led us to consider the possibility that EVM053 can also catalyze the reduction of arsenate species. By substituting DMA-5 as the electron acceptor in the standard glutaredoxin assay,[53] we have demonstrated significant increases in GSSG production that depend on the presence of EVM053 in a concentration-dependent manner. The arsenate reductase activities for hGSTO1-1 and hGSTO2-2, have been reported as 0.15 and 0.03 μmol NADPH oxidized/min per mg protein, respectively, when using 10 mM DMA-5 as substrate.[51] At the same substrate concentration, EVM053 reduces DMA-5 with an activity of approximately 0.25 μmol NADPH oxidized/min per mg protein. A full biochemical characterization of EVM053 as a reducing agent for arsenic species will be published elsewhere.

The arsenate reductase from *E. coli*, ArsC, has been reported to share structural homology with glutaredoxin and GSTs.[54] The catalytic cysteine (Cys12) of ArsC corresponds to Cys23 of EVM053, and thiolate stabilization lowers its pK_a value to 6.4.[55] Interestingly, catalysis by ArsC requires the presence of both GSH and glutaredoxin.[56] Structures of ArsC in complex with arsenate and arsenite have implicated a mechanism involving a glutathionylated ArsC-Cys12-S-As(OOH)-SG intermediate. Deglutathionylation of this intermediate by glutaredoxin is proposed to form the observed ArsC-Cys12-As^{+}-OH thiarsahydroxy intermediate.[54] However, dimethylated arsenic cannot form such a cationic intermediate, and EVM053-catalyzed DMA-5 reduction must therefore use a different mechanism.

Conclusions

The high-resolution crystal structures of oxidized and reduced EVM053 show close resemblance to Grx-1 structures from human and pig in both tertiary structure and active site geometry. However, there are discrete differences that may reflect evolutionary adaptations to the viral life cycle. Most importantly, we have observed a redox-correlated structural change in the loop preceding the active site that greatly affects the conformation and solvent accessibility of Tyr21. This change is not seen in a comparison of reduced human Grx-1 with oxidized pig Grx-1. Moreover, all orthopoxviruses conserve an aromatic residue at this position, whereas mammalian Grx-1 orthologs conserve a proline. This suggests that the rearrangement of Tyr21 is a virus-specific adaptation, possibly affecting substrate specificity or increasing redox potential. In contrast, the redox-correlated conformational change of Thr22 is observed for both orthopoxviral and mammalian Grx-1. Since Thr22 can form hydrogen bonds with the side-chain of the highly conserved Lys20, the redox-induced conformational change may play a mechanistic role in catalysis by both the poxviral and mammalian enzymes. A second orthopox-specific feature is the conservation of a proline at position 53. In EVM053 this proline adopts an energetically strained *cis*-peptide conformation, which changes the conformation of the loop following the second β-strand. In *E. coli* Grx-1 this loop interacts with the bound C-terminal peptide of the RNR-R1 subunit. We propose that this loop is also important for RNR reduction by mammalian and orthopoxviral Grx-1. As a third viral adaptation we suggest that the replacement of three non-catalytic cysteine residues that are conserved in many mammalian Grx-1 sequences prevents enzyme inhibition in oxidizing environments. Both the Tyr21 conformational change and the cysteine replacements may be adaptations to an oxidative environment in virosomes that results from high RNR activity. Finally, the observation of an EVM053-DMA complex and the known ability of the glutaredoxin-like omega GSTs to reduce pentavalent arsenic species led us to the finding of dimethylarsenate reductase activity in EVM053. Our study has generated several new structure-based hypotheses of glutaredoxin function. We are now using mutagenesis and biochemical assays to evaluate these hypotheses and to separate features that are specific to the poxviral enzymes from those that are shared by glutaredoxins in general.

Materials and Methods

Cloning, expression, purification and crystallization

The cloning, expression, purification and crystallization of EVM053 has been described.[57] Briefly, the purified protein was concentrated to 8–10 mg ml^{-1} in a solution

containing 10 mM Tris (pH 8.0) and 100 mM NaCl. DTT was added to a final concentration of 5 mM immediately prior to crystallization. Crystals were grown at 295 K in 24-well plates using the hanging-drop vapour-diffusion method. Crystals suitable for X-ray diffraction were obtained from a reservoir solution containing 20% MPD and 0.1 M sodium cacodylate (pH 6.0) or 12.5% MPD and 0.1 M sodium cacodylate (pH 5.2). The former crystals were flash cooled directly in liquid nitrogen and yielded the structure in the oxidized state. The latter crystals were soaked for 5 min, just before flash cooling, in a solution containing reservoir solution, 50 mM GSH, and 40% MPD, to yield the structure in the reduced state.

We noted that the simultaneous presence of DTT and DMA5 was required for crystal growth and that these compounds induced immediate precipitate formation. The precipitate would remain after crystals had grown and formed a thick film at the surface of the drop to which the crystals would often be attached. With other buffers or reducing agents precipitate formation was temporary or did not occur at all. DTT is known to reduce DMA-5 to trivalent dimethylarsenite (DMA-3), forming oxidized DTT and stable DMA-3-DTT adducts. The formation of crystals of EVM053 in the oxidized state from a solution containing 5 mM reduced DTT suggests that cacodylate led to the oxidation of EVM053, either indirectly by forming oxidized DTT, or directly by EVM053-catalyzed reduction of cacodylate. Oxidized DTT may also have contributed to precipitate formation by cross-linking the two accessible protein thiols, Cys23 and Cys108.

Data collection

Data were collected at 100K on beamline 8.3.1 of the Advanced Light Source (ALS) at Lawrence Berkeley Laboratory using an ADSC Quantum 210 CCD detector. Diffraction data were integrated with MOSFLM[58] followed by scaling and merging with SCALA from the CCP4 suite of programs.[59]

Structure determination and refinement

The EVM053 structure was solved by molecular replacement using the program PHASER[60] and a search model based on the pig liver Grx-1 crystal structure.[19] The initial model was built by ARP/wARP[61] based on the pig liver Grx-1 structural template. Refinement was performed using REFMAC[62] using standard protocols with 5% of the data omitted to monitor R_{free}. Non-crystallographic symmetry restraints were always applied and a TLS atomic displacement model[63] was used in the later stages of refinement. The occupancy of residues with dual side-chain conformations was refined by SHELXL.[64] Water molecules were automatically added using ARP/wARP followed by visual inspection with Xfit.[65] Xfit was also used for manual model building and structure analysis. Stereochemical quality of the final models was assessed by PROCHECK.[16] All structural alignments were performed using DaliLite.[66]

Arsenate reductase assays

Glutaredoxin activity assays were carried out essentially as described.[12] Briefly, a 100 μl reaction mixture contained 100 mM Tris (pH 6.8), 5 mM EDTA, 0.35 mM NADPH, 1 mM GSH, 0.2 units GSH reductase (Sigma) and appropriate dilutions of purified EVM053. Assays were performed at room temperature. Enzyme activity was first confirmed using 2 mM L-cystine as the electron-accepting substrate. Arsenate reductase activity was determined by substituting 10 mM DMA-5 as the electron acceptor. Reactions were monitored spectrophotometrically at 340 nm for 3 min starting 30 s after addition of enzyme. Absorption decrease was linear during this time period. Reaction rates were corrected for the spontaneous rate in absence of enzyme and the result expressed as the formation of micromoles of $NADP^+$/min per mg of enzyme.

Protein Data Bank accession codes

Atomic coordinates for reduced and oxidized EVM053 have been deposited in the RCSB Protein Data Bank with accession codes 2HZE and 2HZF, respectively.

Acknowledgements

We thank L. Price for assistance in crystallization and Dr J. Holton for support with data collection. Ectromelia DNA was kindly provided by Dr M. Barry. X-ray diffraction data were collected at beamline 8.3.1 of the Advanced Light Source (ALS) at Lawrence Berkeley Laboratory, under an agreement with the Alberta Synchroton Institute (ASI). The ALS is operated by the Department of Energy and supported by the National Institute of Health. Beamline 8.3.1 was funded by the National Science Foundation, the University of California and Henry Wheeler. The ASI synchrotron access program is supported by grants from the Alberta Science and Research Authority (ASRA) and the Alberta Heritage Foundation for Medical Research (AHFMR). This research was funded through a grant by the Protein Engineering Network of Centres of Excellence. B.H. is an AHFMR Scholar.

References

1. Fernandes, A. P. & Holmgren, A. (2004). Glutaredoxins: glutathione-dependent redox enzymes with functions far beyond a simple thioredoxin backup system. *Antioxid. Redox Signal.* **6**, 63–74.
2. Krause, G., Lundstrom, J., Barea, J. L., Pueyo de la Cuesta, C. & Holmgren, A. (1991). Mimicking the active site of protein disulfide-isomerase by substitution of proline 34 in *Escherichia coli* thioredoxin. *J. Biol. Chem.* **266**, 9494–9500.
3. Aslund, F., Berndt, K. D. & Holmgren, A. (1997). Redox potentials of glutaredoxins and other thiol-disulfide oxidoreductases of the thioredoxin superfamily determined by direct protein-protein redox equilibria. *J. Biol. Chem.* **272**, 30780–30786.
4. Jung, C. H. & Thomas, J. A. (1996). S-glutathiolated hepatocyte proteins and insulin disulfides as substrates for reduction by glutaredoxin, thioredoxin, protein disulfide isomerase, and glutathione. *Arch. Biochem. Biophys.* **335**, 61–72.
5. Holmgren, A. (1976). Hydrogen donor system for *Escherichia coli* ribonucleoside-diphosphate reductase

dependent upon glutathione. *Proc. Natl Acad. Sci. USA*, **73**, 2275–2279.
6. Mukhopadhyay, R. & Rosen, B. P. (2002). Arsenate reductases in prokaryotes and eukaryotes. *Environ. Health Perspect.* **110**(Suppl. 5), 745–748.
7. Gravina, S. A. & Mieyal, J. J. (1993). Thioltransferase is a specific glutathionyl mixed disulfide oxidoreductase. *Biochemistry*, **32**, 3368–3376.
8. Shelton, M. D., Chock, P. B. & Mieyal, J. J. (2005). Glutaredoxin: role in reversible protein s-glutathionylation and regulation of redox signal transduction and protein translocation. *Antioxid. Redox Signal.* **7**, 348–366.
9. Moss, B. (2001). Poxviruses. In *Fields Virology* 4th edit. (Knipe, D. M., Howley, D. E., Griffin, R. A., Lamb, M. A., Martin, B. & Roizman Straus, S. E., eds), vol. 2, pp. 2849–2884. Lippincott Williams and Wilkins, Philadelphia.
10. White, C. L., Weisberg, A. S. & Moss, B. (2000). A glutaredoxin, encoded by the G4L gene of vaccinia virus, is essential for virion morphogenesis. *J. Virol.* **74**, 9175–9183.
11. Su, H. P., Lin, D. Y. & Garboczi, D. N. (2006). The structure of G4, the poxvirus disulfide oxidoreductase essential for virus maturation and infectivity. *J. Virol.* **80**, 7706–7713.
12. Ahn, B. Y. & Moss, B. (1992). Glutaredoxin homolog encoded by vaccinia virus is a virion-associated enzyme with thioltransferase and dehydroascorbate reductase activities. *Proc. Natl Acad. Sci. USA*, **89**, 7060–7064.
13. Rajagopal, I., Ahn, B. Y., Moss, B. & Mathews, C. K. (1995). Roles of vaccinia virus ribonucleotide reductase and glutaredoxin in DNA precursor biosynthesis. *J. Biol. Chem.* **270**, 27415–27418.
14. Delaroque, N., Muller, D. G., Bothe, G., Pohl, T., Knippers, R. & Boland, W. (2001). The complete DNA sequence of the *Ectocarpus siliculosus* virus EsV-1 genome. *Virology*, **287**, 112–132.
15. Marcotte, E. M., Pellegrini, M., Ng, H. L., Rice, D. W., Yeates, T. O. & Eisenberg, D. (1999). Detecting protein function and protein-protein interactions from genome sequences. *Science*, **285**, 751–753.
16. Laskowski, R. A., MacArthur, M. W., Moss, D. S. & Thornton, J. M. (1993). PROCHECK: a program to check the stereochemical quality of protein structures. *J. Appl. Crystallog.* **26**, 283–291.
17. Nordstrand, K., slund, F., Holmgren, A., Otting, G. & Berndt, K. D. (1999). NMR structure of *Escherichia coli* glutaredoxin 3-glutathione mixed disulfide complex: implications for the enzymatic mechanism. *J. Mol. Biol.* **286**, 541–552.
18. Berardi, M. J. & Bushweller, J. H. (1999). Binding specificity and mechanistic insight into glutaredoxin-catalyzed protein disulfide reduction. *J. Mol. Biol.* **292**, 151–161.
19. Katti, S. K., Robbins, A. H., Yang, Y. & Wells, W. W. (1995). Crystal structure of thioltransferase at 2.2 A resolution. *Protein Sci.* **4**, 1998–2005.
20. Burmeister, W. P. (2000). Structural changes in a cryo-cooled protein crystal owing to radiation damage. *Acta Crystallog. sect. D*, **56**, 328–341.
21. Guddat, L. W., Bardwell, J. C. & Martin, J. L. (1998). Crystal structures of reduced and oxidized DsbA: investigation of domain motion and thiolate stabilization. *Structure*, **6**, 757–767.
22. Lennon, B. W., Williams, C. H., Jr & Ludwig, M. L. (1999). Crystal structure of reduced thioredoxin reductase from *Escherichia coli*: structural flexibility in the isoalloxazine ring of the flavin adenine dinucleotide cofactor. *Protein Sci.* **8**, 2366–2379.
23. Conway, M. E., Yennawar, N., Wallin, R., Poole, L. B. & Hutson, S. M. (2002). Identification of a peroxide-sensitive redox switch at the CXXC motif in the human mitochondrial branched chain aminotransferase. *Biochemistry*, **41**, 9070–9078.
24. Nordstrand, K., Aslund, F., Meunier, S., Holmgren, A., Otting, G. & Berndt, K. D. (1999). Direct NMR observation of the Cys-14 thiol proton of reduced *Escherichia coli* glutaredoxin-3 supports the presence of an active site thiol-thiolate hydrogen bond. *FEBS Letters*, **449**, 196–200.
25. Maignan, S., Guilloteau, J. P., Zhou-Liu, Q., Clement-Mella, C. & Mikol, V. (1998). Crystal structures of the catalytic domain of HIV-1 integrase free and complexed with its metal cofactor: high level of similarity of the active site with other viral integrases. *J. Mol. Biol.* **282**, 359–368.
26. Yang, Y., Jao, S., Nanduri, S., Starke, D. W., Mieyal, J. J. & Qin, J. (1998). Reactivity of the human thioltransferase (glutaredoxin) C7S, C25S, C78S, C82S mutant and NMR solution structure of its glutathionyl mixed disulfide intermediate reflect catalytic specificity. *Biochemistry*, **37**, 17145–17156.
27. Bushweller, J. H., Billeter, M., Holmgren, A. & Wuthrich, K. (1994). The nuclear magnetic resonance solution structure of the mixed disulfide between *Escherichia coli* glutaredoxin(C14S) and glutathione. *J. Mol. Biol.* **235**, 1585–1597.
28. Hazes, B. & Dijkstra, B. W. (1988). Model building of disulfide bonds in proteins with known three-dimensional structure. *Protein Eng.* **2**, 119–125.
29. Guddat, L. W., Bardwell, J. C., Glockshuber, R., Huber-Wunderlich, M., Zander, T. & Martin, J. L. (1997). Structural analysis of three His32 mutants of DsbA: support for an electrostatic role of His32 in DsbA stability. *Protein Sci.* **6**, 1893–1900.
30. Eklund, H., Ingelman, M., Soderberg, B. O., Uhlin, T., Nordlund, P., Nikkola, M. *et al.* (1992). Structure of oxidized bacteriophage T4 glutaredoxin (thioredoxin). Refinement of native and mutant proteins. *J. Mol. Biol.* **228**, 596–618.
31. Sun, C., Berardi, M. J. & Bushweller, J. H. (1998). The NMR solution structure of human glutaredoxin in the fully reduced form. *J. Mol. Biol.* **280**, 687–701.
32. Jao, S. C., English Ospina, S. M., Berdis, A. J., Starke, D. W., Post, C. B. & Mieyal, J. J. (2006). Computational and mutational analysis of human glutaredoxin (thioltransferase): probing the molecular basis of the low pKa of cysteine 22 and its role in catalysis. *Biochemistry*, **45**, 4785–4796.
33. Srinivasan, U., Mieyal, P. A. & Mieyal, J. J. (1997). pH profiles indicative of rate-limiting nucleophilic displacement in thioltransferase catalysis. *Biochemistry*, **36**, 3199–3206.
34. Rabenstein, D. L. & Millis, K. K. (1995). Nuclear magnetic resonance study of the thioltransferase-catalyzed glutathione/glutathione disulfide interchange reaction. *Biochim. Biophys. Acta*, **1249**, 29–36.
35. Johansson, C., Lillig, C. H. & Holmgren, A. (2004). Human mitochondrial glutaredoxin reduces S-glutathionylated proteins with high affinity accepting electrons from either glutathione or thioredoxin reductase. *J. Biol. Chem.* **279**, 7537–7543.
36. Whitesides, G. M., Houk, I. & Patterson, M. A. K. (1983). Activation parameters for thiolate-disulfide interchange reactions in aqueous solution. *J. Organ. Chem.* **48**, 112–115.

37. Armstrong, R. N. (1997). Structure, catalytic mechanism, and evolution of the glutathione transferases. *Chem. Res. Toxicol.* **10**, 2–18.
38. Lycksell, P. O., Ingemarson, R., Davis, R., Graslund, A. & Thelander, L. (1994). ^{1}H NMR studies of mouse ribonucleotide reductase: the R2 protein carboxyl-terminal tail, essential for subunit interaction, is highly flexible but becomes rigid in the presence of protein R1. *Biochemistry*, **33**, 2838–2842.
39. Hopper, S., Johnson, R. S., Vath, J. E. & Biemann, K. (1989). Glutaredoxin from rabbit bone marrow. Purification, characterization, and amino acid sequence determined by tandem mass spectrometry. *J. Biol. Chem.* **264**, 20438–20447.
40. Padilla, C. A., Martinez-Galisteo, E., Barcena, J. A., Spyrou, G. & Holmgren, A. (1995). Purification from placenta, amino acid sequence, structure comparisons and cDNA cloning of human glutaredoxin. *Eur. J. Biochem.* **227**, 27–34.
41. Wang, Y., Amegbey, G. & Wishart, D. S. (2004). Solution structures of reduced and oxidized bacteriophage T4 glutaredoxin. *J. Biomol. NMR*, **29**, 85–90.
42. Nordstrand, K., Sandstrom, A., Aslund, F., Holmgren, A., Otting, G. & Berndt, K. D. (2000). NMR structure of oxidized glutaredoxin 3 from *Escherichia coli*. *J. Mol. Biol.* **303**, 423–432.
43. Doublie, S., Tabor, S., Long, A. M., Richardson, C. C. & Ellenberger, T. (1998). Crystal structure of a bacteriophage T7 DNA replication complex at 2.2 A resolution. *Nature*, **391**, 251–258.
44. Schramm, B. & Locker, J. K. (2005). Cytoplasmic organization of POXvirus DNA replication. *Traffic*, **6**, 839–846.
45. Elledge, S. J., Zhou, Z. & Allen, J. B. (1992). Ribonucleotide reductase: regulation, regulation, regulation. *Trends Biochem. Sci.* **17**, 119–123.
46. Davis, R. E. (1992). Ph. D. thesis. Oregon State University, Corvallis, OR.
47. Padilla, C. A., Spyrou, G. & Holmgren, A. (1996). High-level expression of fully active human glutaredoxin (thioltransferase) in *E. coli* and characterization of Cys7 to Ser mutant protein. *FEBS Letters*, **378**, 69–73.
48. Klintrot, I. M., Hoog, J. O., Jornvall, H., Holmgren, A. & Luthman, M. (1984). The primary structure of calf thymus glutaredoxin. Homology with the corresponding *Escherichia coli* protein but elongation at both ends and with an additional half-cystine/cysteine pair. *Eur. J. Biochem.* **144**, 417–423.
49. Balassu, T. C. & Robinson, A. J. (1987). Orf virus replication in bovine testis cells: kinetics of viral DNA, polypeptide, and infectious virus production and analysis of virion polypeptides. *Arch. Virol.* **97**, 267–281.
50. Chouchane, S. & Snow, E. T. (2001). In vitro effect of arsenical compounds on glutathione-related enzymes. *Chem. Res. Toxicol.* **14**, 517–522.
51. Schmuck, E. M., Board, P. G., Whitbread, A. K., Tetlow, N., Cavanaugh, J. A., Blackburn, A. C. & Masoumi, A. (2005). Characterization of the monomethylarsonate reductase and dehydroascorbate reductase activities of Omega class glutathione transferase variants: implications for arsenic metabolism and the age-at-onset of Alzheimer's and Parkinson's diseases. *Pharmacogenet. Genomics*, **15**, 493–501.
52. Board, P. G., Coggan, M., Chelvanayagam, G., Easteal, S., Jermiin, L. S., Schulte, G. K. *et al.* (2000). Identification, characterization, and crystal structure of the Omega class glutathione transferases. *J. Biol. Chem.* **275**, 24798–24806.
53. Holmgren, A. & Aslund, F. (1995). Glutaredoxin. *Methods Enzymol.* **252**, 283–292.
54. Martin, P., DeMel, S., Shi, J., Gladysheva, T., Gatti, D. L., Rosen, B. P. & Edwards, B. F. (2001). Insights into the structure, solvation, and mechanism of ArsC arsenate reductase, a novel arsenic detoxification enzyme. *Structure*, **9**, 1071–1081.
55. Gladysheva, T., Liu, J. & Rosen, B. P. (1996). His-8 lowers the pKa of the essential Cys-12 residue of the ArsC arsenate reductase of plasmid R773. *J. Biol. Chem.* **271**, 33256–33260.
56. Liu, J. & Rosen, B. P. (1997). Ligand interactions of the ArsC arsenate reductase. *J. Biol. Chem.* **272**, 21084–21089.
57. Bacik, J. P., Brigley, A. M., Channon, L. D., Audette, G. F. & Hazes, B. (2005). Purification, crystallization and preliminary diffraction studies of an ectromelia virus glutaredoxin. *Acta Crystallog. sect. F*, **61**, 550–552.
58. Leslie, A. G. (2006). The integration of macromolecular diffraction data. *Acta Crystallog. sect. D*, **62**, 48–57.
59. Collaborative Computational Project, Number 4. (1994). The CCP4 suite: programs for protein crystallography. *Acta Crystallog. sect. D*, **50**, 760–763.
60. McCoy, A. J., Grosse-Kunstleve, R. W., Storoni, L. C. & Read, R. J. (2005). Likelihood-enhanced fast translation functions. *Acta Crystallog. sect. D*, **61**, 458–464.
61. Perrakis, A., Harkiolaki, M., Wilson, K. S. & Lamzin, V. S. (2001). ARP/wARP and molecular replacement. *Acta Crystallog. sect. D*, **57**, 1445–1450.
62. Murshudov, G. N., Vagin, A. A. & Dodson, E. J. (1997). Refinement of macromolecular structures by the maximum-likelihood method. *Acta Crystallog. sect. D*, **53**, 240–255.
63. Winn, M. D., Isupov, M. N. & Murshudov, G. N. (2001). Use of TLS parameters to model anisotropic displacements in macromolecular refinement. *Acta Crystallog. sect. D*, **57**, 122–133.
64. Sheldrick, G. M. (1997). *SHELXL-97* Program for crystal structure refinement. Inst. Fur Anorganische chemie, Universitat Gottingen, Germany.
65. McRee, D. E. (1999). XtalView/Xfit–A versatile program for manipulating atomic coordinates and electron density. *J. Struct. Biol.* **125**, 156–165.
66. Holm, L. & Park, J. (2000). DaliLite workbench for protein structure comparison. *Bioinformatics*, **16**, 566–567.
67. Kraulis, P. J. (1991). MOLSCRIPT: a program to produce both detailed and schematic plots of protein structures. *J. Appl. Crystallog.* **24**, 946–950.
68. Merritt, E. A. & Murphy, M. E. (1994). Raster3D Version 2.0. A program for photorealistic molecular graphics. *Acta Crystallog. sect. D*, **50**, 869–873.
69. DeLano, W. L. (2002). The PyMOL Molecular Graphics System. DeLano Scientific, San Carlos, CA.

Edited by R. Huber

(Received 16 August 2006; received in revised form 20 October 2006)
Available online 6 November 2006